The Journal of Chemical Physics

High resolution spectral analysis of oxygen. IV. Energy levels, partition sums, band constants, RKR potentials, Franck-Condon factors involving the $X^3\Sigma_g^-$, $a^1\Delta_g$ and $b^1\Sigma_g^+$ states

Cite as: J. Chem. Phys. **141**, 174302 (2014); https://doi.org/10.1063/1.4900510
Submitted: 11 September 2014 . Accepted: 09 October 2014 . Published Online: 03 November 2014

Shanshan Yu, Brian J. Drouin, and Charles E. Miller

High resolution spectral analysis of oxygen. IV. Energy levels, partition sums, band constants, RKR potentials, Franck-Condon factors involving the $X^3\Sigma_g^-$, $a^1\Delta_g$ and $b^1\Sigma_g^+$ states

Shanshan Yu,[a] Brian J. Drouin, and Charles E. Miller
Jet Propulsion Laboratory, California Institute of Technology, Pasadena, California 91109, USA

(Received 11 September 2014; accepted 9 October 2014; published online 3 November 2014)

We have updated the isotopically invariant Dunham fit of O_2 with newly reported literature transitions to derive (1) the energy levels, partition sums, band-by-band molecular constants, and RKR potentials for the $X^3\Sigma_g^-$, $a^1\Delta_g$, and $b^1\Sigma_g^+$ states of the six O_2 isotopologues: $^{16}O^{16}O$, $^{16}O^{17}O$, $^{16}O^{18}O$, $^{17}O^{17}O$, $^{17}O^{18}O$, and $^{18}O^{18}O$; (2) Franck-Condon factors for their $a^1\Delta_g - X^3\Sigma_g^-$, $b^1\Sigma_g^+ - X^3\Sigma_g^-$, and $a^1\Delta_g - b^1\Sigma_g^+$ band systems. This new spectroscopic parameterization characterizes all known transitions within and between the $X^3\Sigma_g^-$, $a^1\Delta_g$, and $b^1\Sigma_g^+$ states within experimental uncertainty and can be used for accurate predictions of as yet unmeasured transitions. All of these results are necessary to provide a consistent linelist of all transitions which will be reported in a followup paper.
 [http://dx.doi.org/10.1063/1.4900510]

I. INTRODUCTION

The molecular physics of oxygen (O_2) are known in exquisite detail due to its fundamental importance in disciplines ranging from astrophysics to biology. It is a first row homonuclear diatomic and a stable diradical with numerous low-lying electronic states, spin-orbit interactions, and allowed transitions. These lead to a rich, complicated spectrum extending from the microwave to the vacuum ultraviolet. Reproducing the molecular properties and associated spectra within experimental accuracy is a rigorous test for quantum theory. Detailed spectroscopic knowledge of O_2 is also essential for the remote sensing of Earth,[1–8] Mars,[9] Venus,[10] and most recently, the insterstellar medium.[11,12]

We initiated a systematic study of the O_2 high resolution transitions within and between the bound electronic states below the $O(^3P) + O(^3P)$ dissociation threshold, motivated by the challenge of developing an accurate and complete spectroscopic characterization of molecular oxygen for current and planned Earth atmospheric observations. Especially, extremely accurate O_2 molecular data are required to fulfill the demand of the proposed 0.3% –1.0% precision for greenhouse gas retrievals by the following spaceborne missions utilizing the O_2 A-band for air mass calibration: the TANSO-FTS on the Japanese Greenhouse Gases Observing satellite (GOSAT),[13] the NASA Orbiting Carbon Observatory re-flight (OCO-2),[14] and the Chinese TanSat satellite instrument.[15] The result of our effort thus far is an isotope-independent Dunham parameterization of the $X^3\Sigma_g^-$, $a^1\Delta_g$, and $b^1\Sigma_g^+$ states which was reported in Papers I–III of this series.[16–18] This "grand fit" to an extensive set of literature experimental data yielded (1) a consistent calibration of the various data sets, (2) characterization of the Born-Oppenheimer Breakdown of the vibronic parameterization, and (3) predictions of O_2 line positions with spectroscopic accuracy.

In the current work, we extend the results of our grand fit involving $X^3\Sigma_g^-$, $a^1\Delta_g$, and $b^1\Sigma_g^+$ to provide a comprehensive list of the rovibronic energy levels, partition sums, band-by-band molecular parameters, RKR potentials and Franck-Condon factors (FCFs). The list of the rovibronic energy levels ties together all of the spectra of a given oxygen isotopologue and governs the thermal partitioning of the states up to high temperatures. To our knowledge no previous works have specifically provided a precise listing of oxygen energy levels. For comparisons of band parameters, we checked our values with the same works as for which the data were extracted, particularly from the most precise sources, e.g., Refs. 17, 19, and 20. The band parameters are useful to readers whose programs are not incorporated with the complicated Dunham model.

Previous *ab initio* work from Bytautas *et al.*[21] provided a solid benchmark for our RKR calculations. A similar *ab initio* benchmark for derived electronic and magnetic properties is provided by Minaev.[22] Frank-Condon factors (FCFs) have been reported multiple times, and some initial discrepancies were more or less cleared up in the NIST report of Nicholls.[23] Here we present comparable values to Nicholls, as well as isotopologue specific values which vary due to minor amounts of Born-Oppenheimer Breakdown in the molecule.

All of the results reported in the current paper are necessary to provide a consistent linelist of all vibronic transitions involving $X^3\Sigma_g^-$, $a^1\Delta_g$, and $b^1\Sigma_g^+$, which will be reported in a followup paper, i.e., Paper V of this series, together with detailed descriptions on intensity calculations with a modified version of our SPCAT software[24] using effective magnetic dipole and quadrupole transition moment operators in a spherical tensor basis. A similar grand fit to experimental data sets involving other higher bound electronic states below the $O(^3P) + O(^3P)$ dissociation threshold is in progress and will be published in Paper VI of this series.

[a]Author to whom correspondence should be addressed: Electronic mail: shanshan.yu@jpl.nasa.gov.

II. MODEL UPDATE

New microwave[17] and infrared[18] measurements have been incorporated into the grand fit for the $X^3\Sigma_g^-$, $a^1\Delta_g$, and $b^1\Sigma_g^+$ states published in Paper I.[16] We added these newly measured positions to our Dunham model and obtained updated molecular constants. The updated fit files, o2.par, o2.lin, and o2.fit, were deposited in the supplementary material.[25] The new microwave measurements[17] involved the pure rotational transitions in the $a^1\Delta_g$ $v = 0$ and 1 states of the six O_2 isotopologues, which helped determine two more hyperfine parameters, the electric quadrupole interaction eQq, and the nuclear spin-rotation interaction C_I. The new infrared measurements[18] included the $(v', v'') = (1,1)$, (2,1), (1,0), (0,1) and (0,0) bands of the $b^1\Sigma_g^+ - X^3\Sigma_g^-$ system for $^{16}O_2$ and the (0,1) and (0,0) bands of the other five O_2 isotopologues. The latter data showed that the $^{17}O^{18}O$ $v' - v'' = 1 - 0$ Raman data of Edwards *et al.*[26] have a 0.2 cm^{-1} calibration error. Paper III[18] resolved discrepancies in Raman data for $^{16}O^{17}O$, $^{17}O^{17}O$, and $^{17}O^{18}O$ and enabled us to improve the vibrational parameterization of the $X^3\Sigma_g^-$ electronic state.

III. ENERGY LEVELS

We calculated energy levels for the $X^3\Sigma_g^-$, $a^1\Delta_g$, and $b^1\Sigma_g^+$ states using the SPCAT software.[24] We employed the molecular constants from the updated grand fit described in Sec. II. Tables S1– S6 in the supplementary material[25] list the energy levels for $^{16}O^{16}O$, $^{16}O^{17}O$, $^{16}O^{18}O$, $^{17}O^{17}O$, $^{17}O^{18}O$, and $^{18}O^{18}O$, respectively, with $v \leq 39$ and $N \leq 65$ for $X^3\Sigma_g^-$, and $v \leq 29$ and $N \leq 65$ for $a^1\Delta_g$ and $b^1\Sigma_g^+$. Four quantum numbers, v, N, J, Λ, are used to describe each rotational level of $^{16}O^{16}O$, $^{16}O^{18}O$, and $^{18}O^{18}O$, where v is for the vibrational momentum; N for the rotational angular momentum; J for the total angular momentum; and Λ for the electron orbital angular momentum. Λ is 2 for all rotational levels of $a^1\Delta_g$, and 0 for those of $X^3\Sigma_g^-$ and $b^1\Sigma_g^+$. The sign in front of Λ is the total parity of each level, and the correlation between the total parity (+/ −) and *e/f* designation follow the recommendation of Brown *et al.*:[27] $p = (-1)^{J+1}$ for *e* levels and $p = (-1)^J$ for *f* levels. Note that the *e/f* levels of each J in $a^1\Delta_g$ have the same energy because no doubling was experimentally observed. Five quantum numbers, v, N, J, Λ, F, are used to describe each rotational level of $^{16}O^{17}O$ and $^{17}O^{18}O$. The additional quantum number F describes the hyperfine structure due to the ^{17}O nuclear spin ($I = \frac{5}{2}$) such that $F = J + 5/2$, $J + 3/2$, $\ldots |J - 5/2|$. Six quantum numbers, v, N, J, Λ, I_{tot}, F, are used to label each rotational level of $^{17}O^{17}O$ with two nuclear spins ($I_1 = I_2 = 5/2$). $I_{tot} = I_1 + I_2$, $I_1 + I_2 - 1. \ldots |I_1 - I_2| = 5, 4, 3, 2, 1, 0$ and $F = J + I_{tot}$, $J + I_{tot} - 1, \ldots |J - I_{tot}|$. Because of the nuclear spin function symmetry, in $X^3\Sigma_g^-$, the even and odd values of N can only be associated with odd and even values of I_{tot}, respectively;[28] in $b^1\Sigma_g^+$, the even and odd values of N can only be associated with even and odd values of I_{tot}, respectively. Without definite parity in the $a^1\Delta_g$ state, both odd and even values of I_{tot} may be associated with a given N, and the even values of I_{tot} are always associated with negative p. It is important to note that all the energies of each isotopologue are shifted by a constant value to be relative to the lowest allowed rotational level in $X^3\Sigma_g^-$ of that isotopologue, i.e., the absolute zero energy is set to the level of $N = 1$ and $J = 0$ for $^{16}O^{16}O$ and $^{18}O^{18}O$, the level of $N = 0$ and $J = 1$ for $^{16}O^{18}O$, the level of $N = 0$, $J = 1$ and $F = 3.5$ for $^{16}O^{17}O$ and $^{17}O^{18}O$, the level of $N = 0$, $J = 1$, $I_{tot} = 5$ and $F = 6$ for $^{17}O^{17}O$.

To the convenience of some readers, Tables S7– S9 in the supplementary material[25] list the hyperfine-free energy levels for $^{16}O^{17}O$, $^{17}O^{17}O$, and $^{17}O^{18}O$. These energies were calculated with the nuclear hyperfine parameters set to zero. In this case, four quantum numbers, v, N, J, Λ, are used to describe each rotational level. The absolute zero energy is set to the level of $N = 1$ and $J = 0$ for $^{17}O^{17}O$, the level of $N = 0$ and $J = 1$ for $^{16}O^{17}O$ and $^{17}O^{18}O$.

The obtained energy levels enable the transition frequency for any line to be calculated by direct subtraction. When compared to HITRAN2012 , frequency differences up to 0.015 cm^{-1} were found for the $^{16}O^{16}O$ $a - X$ system, up to 0.05 cm^{-1} for $^{16}O^{16}O$ $b - X$, up to 0.05 cm^{-1} for $^{16}O^{17}O$ $a - X$, up to 0.025 cm^{-1} for $^{16}O^{17}O$ $b - X$, up to 0.003 cm^{-1} for $^{16}O^{18}O$ $a - X$, up to 0.09 cm^{-1} for $^{16}O^{18}O$ $b - X$. Figure 1 shows the differences between listed frequencies labeled by the quantum number J'' plotted versus line intensity for the (upper) transitions within the X ground state, (middle) transitions between the ground and the $^1\Delta$ state ($a - X$), and (lower) transitions between the ground and the $^1\Sigma$ state ($b - X$). The colors are chosen to highlight the sub-bands within each electronic series. Solid horizontal patches indicate that agreement across different intensities is good.

The frequencies of the calculated pure rotational transitions for $X(0) - X(0)$ are in quite close agreement with HITRAN2012[29] with no pattern emerging from the red difference points (residual = ν(this work) - ν(HITRAN2012)) in the upper panel of Figure 1 for transitions with intensities greater than 3×10^{-28} cm^{-1}/molecule cm^{-2}. Below this intensity a small tail (< 0.0025 cm^{-1}) due to extrapolative differences is observed. The frequencies for $X(1) - X(1)$ show a general pattern of positive residuals for the strongest transitions and a tail extending to negative residuals for the weaker transitions. Again, the residuals are small and reflect minor changes in the spectral parameters.

The frequencies of the vibrational transitions are also different in comparison with the HITRAN2012 linelist. The orange data points in the upper panel show a J-dependent pattern that becomes more negative (approaching −0.005 cm^{-1} in going from the lowest J transitions towards the most intense transitions, after which the relative difference decreases and even becomes slightly positive for some of the highest J transitions listed. It is interesting to point out that the energy levels among the $v = 0,1$ states are exactly the same in our listing, and that the frequency differences for the pure rotational transitions are all significantly smaller than those for these vibrational transitions. If we were comparing two models, one may expect the vibrational transition frequencies to have related J-dependences, but this is clearly not the case depicted in Figure 1. We attribute this situation to the fact that HITRAN, in general, is a compilation from multiple sources

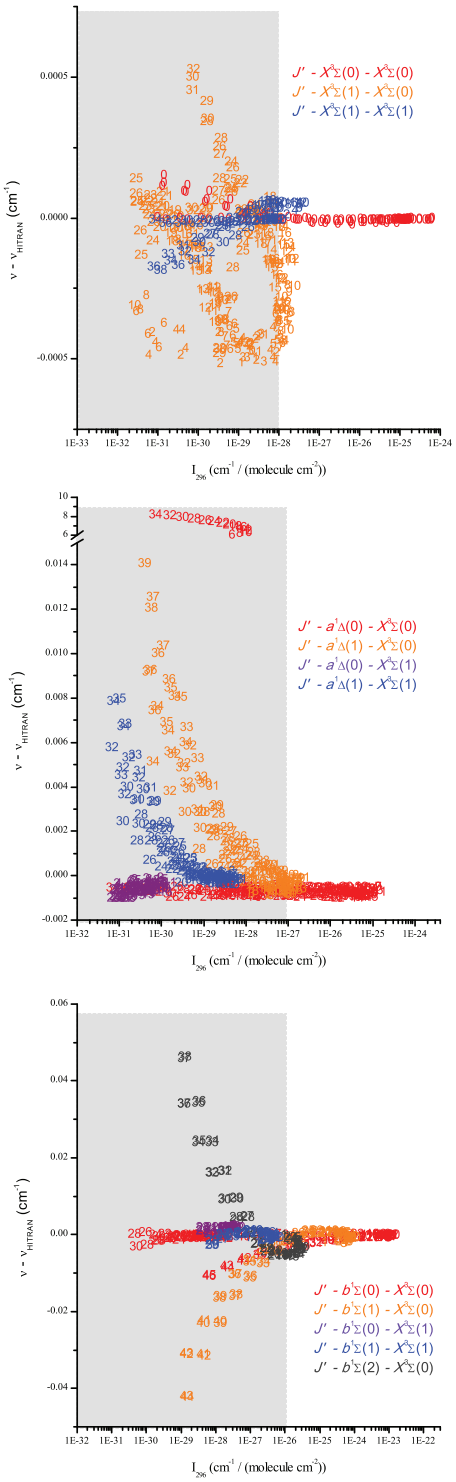

FIG. 1. Comparisons of the predicted $^{16}O^{16}O$ positions versus the HITRAN 2012 compilation. The panels show differences between listed frequencies labeled by the quantum number J'' plotted vs. line intensity for the transitions within the X ground state (upper), the atmospheric IR $a^1\Delta_g - X^3\Sigma_g^-$ system around 8000 cm^{-1} (middle) and the atmospheric $b^1\Sigma_g^+ - X^3\Sigma_g^-$ system around 13000 cm^{-1} (lower) electronic transitions.

and that the models from one band to the next are not necessarily common to each other.

Comparisons of the positions for $a^1\Delta_g(v')$ - $X^3\Sigma_g^-(v'')$ reveal only minor deviations of the frequencies from the HITRAN2012 listing (< 0.014 cm^{-1} at the weakest transitions for the (0,1) vibronic state) except for a single sub-branch of the (0,0) state which deviates by 6-10 cm^{-1}. Inspection of the sub-branch revealed an inconsistency in the HITRAN energy levels indicating that an inappropriate pair of levels was utilized in the calculation of the transition frequencies. It was found that in HITRAN2012, the quantum numbers for the $^{\Delta N}\Delta J{=}^P O$ branch of the $^{16}O^{16}O$ $a - X\,(v', v'') = (0, 0)$ band were incorrectly labeled, i.e., the 7875.6 cm^{-1} transition with a lower state energy of 16.4 cm^{-1} was labeled as $N'' = 1$ and $J'' = 2$. This label indicates $N' = 0$ and $J' = 0$, but the rotational level of $N' = 0$ and $J' = 0$ does not exist in the $a^1\Delta_g$ state. The correct assignment for this line is $N'' = 3$ and $J'' = 4$. Other lines in the same $^P O$ branch were also incorrectly labeled with the same shift of 2 in quantum numbers.

For the $b^1\Sigma_g^+(v')$ - $X^3\Sigma_g^-(v'')$ system, deviations of the frequencies are minor for the $(v', v'') = (0, 0), (0, 1)$, and (1, 1) bands. The orange data points in the lower panel show a J-dependent pattern that becomes negative and approaches -0.04 cm^{-1} for (1,0). The black data points show a J-dependent pattern that becomes positive and approaches 0.05 cm^{-1} for (1,1).

IV. PARTITION SUMS

As a prerequisite for the prediction of rovibronic transition intensities, we calculated the total partition sums of the oxygen isotopologues. The SPCAT program produces output based on a direct sum-over states of all energy levels calculated with their respective degeneracies:

$$Q_{evsr} = \sum_i d_i e^{-E_i/kT}, \tag{1}$$

where the subscript $evsr$ indicates that the summation includes contributions from e electronic states—X, a, b; from v vibrational states—$X(v < 35)$, $a(v < 20)$, and $b(v < 20)$; from s spin states—$S(X) = 1$, $I(^{17}O) = \frac{5}{2}$; and from r rotational states up to $J = 99$. Note that the degeneracy of the orbital angular momentum in the a state is counted by keeping the parity labels distinct and thus producing accidentally degenerate pairs of energy levels for each J. Note that the absolute zero energy of each isotopologue is set to the lowest allowed rotational level in its $X^3\Sigma_g^-$ state as discussed in Sec. III. Table I reports values of Q_{evsr} for temperatures from 9 to 300 K and show the expected dependences on symmetry, mass and spin. Comparison with TIPS[30] reveals an additive systematic error of almost exactly 3 for $^{16}O^{18}O$ and nearly 18 for $^{16}O^{17}O$. For $^{16}O^{18}O$ this is the degeneracy of the $N = 0$ level at zero energy, and for $^{16}O^{17}O$ 18 is the sum of the degeneracies for the three hyperfine levels associated with $N = 0$. For $^{16}O_2$, the $N = 0$ level does not exist. We confirmed the starting energy level error in TIPS[31] and regenerated the summations using the energy levels from our model. Further comparisons of our Q_{evsr} values revealed inconsistencies beyond the fifth significant figure due to dated values of fundamental constants in the program codes. The Boltzmann constant utilized for partition sum calculations in SPCAT was updated to the 2010 CODATA value 0.69503476(63) cm^{-1}/K.[32] The TIPS compilation will be similarly updated[31] and available through

TABLE I. Partition sums, Q_{evsr} for oxygen isotopologues with no hyperfine splittings.

Temperature	$^{16}O_2$	$^{16}O^{18}O$	$^{16}O^{17}O$	$^{17}O_2$	$^{17}O^{18}O$	$^{18}O_2$
300.000	218.6562	461.4189	449.0513	463.0775	476.2471	245.6074
296.000	215.7364	455.2301	443.0315	456.8660	469.8553	242.3158
225.000	164.0601	345.7514	336.5179	346.9895	356.8186	184.1223
150.000	109.6050	230.4320	224.2984	231.2544	237.7826	122.8567
75.000	55.1979	115.2150	112.1761	115.6224	118.8558	61.6498
37.500	28.0345	57.6805	56.1870	57.8807	59.4689	31.0876
18.750	14.5149	29.0178	28.2941	29.1148	29.8835	15.8675
9.375	7.8713	14.8627	14.5186	14.9087	15.2733	8.3676

the HITRAN database.[29] Table II reports values of Q_{evsr} for oxygen isotopologues with the nuclear hyperfine splittings.

V. BAND PARAMETERS

We calculated spectroscopic parameters and their uncertainties for each vibronic state using the grand fit results, their uncertainties, and the associated parameter correlation matrix obtained from the updated Dunham model described in Sec. II. Table III lists the vibrational, rotational, and centrifugal distortion constants for the $X^3\Sigma_g^-$, $a^1\Delta_g$ and $b^1\Sigma_g^+$ states of $^{16}O^{16}O$. Tables IV and V list the spin-splitting and spin-rotation constants for the $X^3\Sigma_g^-$ state of $^{16}O^{16}O$. For all numbers in Tables III–V, we keep more decimals than experimentally determined uncertainties to avoid numerical round-off errors. The band constants for the minor isotopologues are deposited in the supplementary material.[25] Tables S10– S12 list the parameters for the $X^3\Sigma_g^-$, $a^1\Delta_g$, and $b^1\Sigma_g^+$ states of all isotopologues, respectively. For the vibrational energies of the $X^3\Sigma_g^-$ state, our fit was obtained for G_v with experimental data over $v = 0 - 23$, and the rotational (B_v, D_v, and H_v), the spin-splitting (λ_v, λ_{Dv}, and λ_{Hv}), and the spin-rotation (γ_v , γ_{Dv} , and γ_{Hv}) parameters were obtained with experimental data over $v = 0 - 23, 26 - 27, 29 - 31$ (see Sec. IV G of Paper I[16] for details). The fitted parameters in the $a^1\Delta_g$ and $b^1\Sigma_g^+$ states were obtained with experimental data over $v = 0 - 10$ and $v = 0 - 12$, respectively. Note that in Table III, all values are derived from our grand fit, except for G_v of the $X^3\Sigma_g^-$ $v = 26 - 27, 29 - 30$ states, which are experimental values with their relative experimental uncertainties. Their absolute experimental uncertainty is 3 cm^{-1} and the observed minus calculated values are −4.3, −9.2, −24.4, −39.9, and −62.6 cm^{-1}, respectively (see Sec. IV G of Paper I[16] for details).

TABLE II. Partition sums, Q_{evsr} for oxygen isotopologues with hyperfine splittings.

Temperature	$^{16}O^{17}O$	$^{17}O_2$	$^{17}O^{18}O$
300.000	2694.2343	8334.9588	2857.4047
296.000	2658.1158	8223.1523	2819.0539
225.000	2019.0354	6245.3807	2140.8357
150.000	1345.7203	4162.1522	1426.6208
75.000	672.9877	2080.7801	713.0616
37.500	337.0536	1041.4318	356.7410
18.750	169.6961	523.6445	179.2289
9.375	87.0417	267.9293	91.5661

Some of the band parameters are not directly comparable to other studies without a few adjustments. For example, T_0 values for the $a^1\Delta_g$ and $b^1\Sigma_g^+$ states, $T_0(a) = 7889.427667(64)$, and $T_0(b) = 13122.2515911(85)$ each differ from literature values[19,33] by an amount equivalent to the difference (0.24584307 cm^{-1}) between the hypothetical $N = 0$ and $J = 1$ level of the $^{16}O^{16}O$ $X^3\Sigma_g^-$ $v = 0$ state and the first allowed level $N = 1$ and $J = 0$. This is simply due to different definitions for the zero point energy. Because of the presence of both levels in the asymmetric isotopologues this offset only occurs in the symmetric cases. In SPFIT a zero point offset energy equivalent to $-(G_0 - E(1, 0))$ is added to all of the energy levels for the symmetric isotopologues whereas the offset is $(G_0 - E(0, 1))$ for the asymmetric isotopologues. For the $a^1\Delta_g$ state, another notable difference of about 6 cm^{-1} arises from the fact that the Hamiltonian in our work contains $[J(J + 1) - \Lambda^2]$ rather than just $J(J + 1)$ as in Leshchishina *et al.*[19]

For the rotational, centrifugal distortion, spin-splitting, and spin-rotation constants, our uncertainties are consistently smaller than those reported by Long *et al.*[34] and Leshchishina *et al.*,[19] i.e., for the $X^3\Sigma_g^-$ state, the determined wavenumber values from our work vs. Long *et al.*[34] vs. Leshchishina *et al.*[19] are: $B_0 = 1.437676035(16)$ vs. 1.437676078(29) vs. 1.437675974(19); $D_0 = 4.840574(57) \times 10^{-6}$ vs. $4.84178(14) \times 10^{-6}$ vs. $4.840356(76) \times 10^{-6}$; $\lambda_0 = 1.984751423(40)$ vs. 1.98475118(5) vs. 1.984751193(50); $\gamma_0 = 8.4253758(29)$ vs. 8.4253696(58) vs. 8.42537356(584).

Another benefit of casting the Dunham parameterization into band parameters is that trends, such as the dramatic increase in λ_v become apparent upon inspection of a tabular listing. The dramatic increase in the ground state spin-splitting parameter at higher v is expected due to the shrinking of the $b - X(v)$ energy gap that governs the effective spin-orbit coupling.[35] Interestingly, it is not a monotonic increase, but instead oscillatory, indicating that at low v, where the spin-orbit coupling is still weak, the changes are likely to be structural, rather than electronic. It is not until above $v = 13$ that the trend becomes monotonic and the stronger spin-orbit coupling dominates the parameter.

VI. RKR POTENTIALS AND FRANCK-CONDON FACTORS

We used Le Roy's RKR1 program[36] and the Dunham-type constants updated in the current work to calculate the RKR potentials of $X^3\Sigma_g^-$, $a^1\Delta_g$, and $b^1\Sigma_g^+$ for each of the six

TABLE III. The vibrational, rotational, and centrifugal distortion constants (in cm^{-1}) for the $X^3\Sigma_g^-$, $a^1\Delta_g$, and $b^1\Sigma_g^+$ states of $^{16}O^{16}O$.

	v	G_v	σG_v	B_v	σB_v	D_v	σD_v	H_v	σH_v
$X^3\Sigma_g^+$	0	$7.870768981385 \times 10^{2}$	3.2×10^{-07}	$1.43767603572 \times 10^{00}$	1.6×10^{-08}	$-4.84057450 \times 10^{-06}$	5.7×10^{-11}	9.655×10^{-14}	2.3×10^{-14}
	1	$2.343466342865 \times 10^{03}$	6.0×10^{-05}	$1.42186583616 \times 10^{00}$	2.5×10^{-07}	$-4.84136115 \times 10^{-06}$	2.1×10^{-10}	3.790×10^{-13}	7.1×10^{-14}
	2	$3.876334352822 \times 10^{03}$	2.7×10^{-04}	$1.40611987207 \times 10^{00}$	7.0×10^{-07}	$-4.84016433 \times 10^{-06}$	5.2×10^{-10}	6.615×10^{-13}	1.1×10^{-13}
	3	$5.385861447181 \times 10^{03}$	6.9×10^{-04}	$1.39042397907 \times 10^{00}$	1.6×10^{-06}	$-4.83793438 \times 10^{-06}$	1.0×10^{-09}	9.440×10^{-13}	1.6×10^{-13}
	4	$6.872209042662 \times 10^{03}$	1.4×10^{-03}	$1.37476784802 \times 10^{00}$	2.8×10^{-06}	$-4.83562169 \times 10^{-06}$	1.7×10^{-09}	1.226×10^{-12}	2.1×10^{-13}
	5	$8.335519168407 \times 10^{03}$	2.6×10^{-03}	$1.35914418581 \times 10^{00}$	4.3×10^{-06}	$-4.83417660 \times 10^{-06}$	2.5×10^{-09}	1.509×10^{-12}	2.6×10^{-13}
	6	$9.775913860209 \times 10^{03}$	3.9×10^{-03}	$1.34354787627 \times 10^{00}$	6.1×10^{-06}	$-4.83454948 \times 10^{-06}$	3.4×10^{-09}	1.791×10^{-12}	3.1×10^{-13}
	7	$1.119349423410 \times 10^{04}$	5.1×10^{-03}	$1.32797514093 \times 10^{00}$	8.1×10^{-06}	$-4.83769068 \times 10^{-06}$	4.4×10^{-09}	2.074×10^{-12}	3.5×10^{-13}
	8	$1.258833923929 \times 10^{04}$	5.9×10^{-03}	$1.31242269994 \times 10^{00}$	1.0×10^{-05}	$-4.84455058 \times 10^{-06}$	5.4×10^{-09}	2.356×10^{-12}	4.0×10^{-13}
	9	$1.396050409046 \times 10^{04}$	6.3×10^{-03}	$1.29688693282 \times 10^{00}$	1.2×10^{-05}	$-4.85607952 \times 10^{-06}$	6.4×10^{-09}	2.639×10^{-12}	4.5×10^{-13}
	10	$1.531001837940 \times 10^{04}$	6.2×10^{-03}	$1.28136303937 \times 10^{00}$	1.4×10^{-05}	$-4.87322787 \times 10^{-06}$	7.4×10^{-09}	2.921×10^{-12}	5.0×10^{-13}
	11	$1.663688386600 \times 10^{04}$	5.8×10^{-03}	$1.26584420045 \times 10^{00}$	1.6×10^{-05}	$-4.89694600 \times 10^{-06}$	8.4×10^{-09}	3.203×10^{-12}	5.4×10^{-13}
	12	$1.794107194864 \times 10^{04}$	5.4×10^{-03}	$1.25032073887 \times 10^{00}$	1.8×10^{-05}	$-4.92818426 \times 10^{-06}$	9.2×10^{-09}	3.486×10^{-12}	5.9×10^{-13}
	13	$1.922252081383 \times 10^{04}$	5.3×10^{-03}	$1.23477928019 \times 10^{00}$	2.0×10^{-05}	$-4.96789301 \times 10^{-06}$	9.9×10^{-09}	3.768×10^{-12}	6.4×10^{-13}
	14	$2.048113226532 \times 10^{04}$	5.6×10^{-03}	$1.21920191354 \times 10^{00}$	2.2×10^{-05}	$-5.01702261 \times 10^{-06}$	1.0×10^{-08}	4.051×10^{-12}	6.9×10^{-13}
	15	$2.171676823252 \times 10^{04}$	5.9×10^{-03}	$1.20356535251 \times 10^{00}$	2.3×10^{-05}	$-5.07652343 \times 10^{-06}$	1.0×10^{-08}	4.333×10^{-12}	7.4×10^{-13}
	16	$2.292924695820 \times 10^{04}$	6.0×10^{-03}	$1.18784009597 \times 10^{00}$	2.3×10^{-05}	$-5.14734583 \times 10^{-06}$	1.1×10^{-08}	4.616×10^{-12}	7.8×10^{-13}
	17	$2.411833886569 \times 10^{04}$	6.1×10^{-03}	$1.17198958885 \times 10^{00}$	2.3×10^{-05}	$-5.23044016 \times 10^{-06}$	1.1×10^{-08}	4.898×10^{-12}	8.3×10^{-13}
	18	$2.528376210529 \times 10^{04}$	7.1×10^{-03}	$1.15596938308 \times 10^{00}$	2.3×10^{-05}	$-5.32675678 \times 10^{-06}$	1.1×10^{-08}	5.181×10^{-12}	8.8×10^{-13}
	19	$2.642517778011 \times 10^{04}$	9.4×10^{-03}	$1.13972629832 \times 10^{00}$	2.3×10^{-05}	$-5.43724607 \times 10^{-06}$	1.0×10^{-08}	5.463×10^{-12}	9.3×10^{-13}
	20	$2.754218485127 \times 10^{04}$	1.2×10^{-02}	$1.12319758288 \times 10^{00}$	2.4×10^{-05}	$-5.56285838 \times 10^{-06}$	1.0×10^{-08}	5.746×10^{-12}	9.7×10^{-13}
	21	$2.863431472241 \times 10^{04}$	1.6×10^{-02}	$1.10631007451 \times 10^{00}$	2.4×10^{-05}	$-5.70454406 \times 10^{-06}$	1.0×10^{-08}	6.028×10^{-12}	1.0×10^{-12}
	22	$2.970102550360 \times 10^{04}$	2.1×10^{-02}	$1.08897936123 \times 10^{00}$	2.6×10^{-05}	$-5.86325349 \times 10^{-06}$	1.1×10^{-08}	6.311×10^{-12}	1.0×10^{-12}
	23	$3.074169595455 \times 10^{04}$	3.3×10^{-02}	$1.07110894223 \times 10^{00}$	2.8×10^{-05}	$-6.03993702 \times 10^{-06}$	1.2×10^{-08}	6.593×10^{-12}	1.1×10^{-12}
	24	$3.175561910719 \times 10^{04}$	6.0×10^{-02}	$1.05258938863 \times 10^{00}$	3.0×10^{-05}	$-6.23554501 \times 10^{-06}$	1.4×10^{-08}	6.876×10^{-12}	1.1×10^{-12}
	25	$3.274199556768 \times 10^{04}$	1.0×10^{-01}	$1.03329750435 \times 10^{00}$	3.2×10^{-05}	$-6.45102782 \times 10^{-06}$	1.7×10^{-08}	7.158×10^{-12}	1.2×10^{-12}
	26	$3.369566103636 \times 10^{04}$	1.2×10^{-02}	$1.01309548696 \times 10^{00}$	3.5×10^{-05}	$-6.68733582 \times 10^{-06}$	2.1×10^{-08}	7.441×10^{-12}	1.2×10^{-12}
	27	$3.461922355942 \times 10^{04}$	1.2×10^{-02}	$9.91830088498 \times 10^{-01}$	3.6×10^{-05}	$-6.94541936 \times 10^{-06}$	2.5×10^{-08}	7.723×10^{-12}	1.3×10^{-12}
	28	$3.552631483325 \times 10^{04}$	4.6×10^{-01}	$9.69331776309 \times 10^{-01}$	3.8×10^{-05}	$-7.22622881 \times 10^{-06}$	3.1×10^{-08}	8.006×10^{-12}	1.3×10^{-12}
	29	$3.636802090462 \times 10^{04}$	1.8×10^{-02}	$9.45413893888 \times 10^{-01}$	4.0×10^{-05}	$-7.53071453 \times 10^{-06}$	3.8×10^{-08}	8.288×10^{-12}	1.4×10^{-12}
	30	$3.718544202131 \times 10^{04}$	1.8×10^{-02}	$9.19871821711 \times 10^{-01}$	4.6×10^{-05}	$-7.85982687 \times 10^{-06}$	4.5×10^{-08}	8.571×10^{-12}	1.4×10^{-12}
	31	$3.796097213336 \times 10^{04}$	2.1×10^{-02}	$8.92482138075 \times 10^{-01}$	6.0×10^{-05}	$-8.21451620 \times 10^{-06}$	5.3×10^{-08}	8.853×10^{-12}	1.5×10^{-12}
	32	$3.878537412792 \times 10^{04}$	1.9×10^{00}	$8.63001779933 \times 10^{-01}$	8.3×10^{-05}	$-8.59573288 \times 10^{-06}$	6.2×10^{-08}	9.136×10^{-12}	1.5×10^{-12}
	33	$3.950904346495 \times 10^{04}$	2.7×10^{00}	$8.31167203731 \times 10^{-01}$	1.1×10^{-04}	$-9.00442727 \times 10^{-06}$	7.2×10^{-08}	9.418×10^{-12}	1.5×10^{-12}
	34	$4.019254850457 \times 10^{04}$	3.6×10^{00}	$7.96693546245 \times 10^{-01}$	1.6×10^{-04}	$-9.44154974 \times 10^{-06}$	8.3×10^{-08}	9.701×10^{-12}	1.6×10^{-12}
	35	$4.083372665956 \times 10^{04}$	4.7×10^{00}	$7.59273785420 \times 10^{-01}$	2.2×10^{-04}	$-9.90805063 \times 10^{-06}$	9.5×10^{-08}	9.983×10^{-12}	1.6×10^{-12}

TABLE III. (*Continued.*)

	v	G_v	σG_v	B_v	σB_v	D_v	σD_v	H_v	σH_v
$a^1\Delta_g$	0	$8.676504565138 \times 10^{03}$	6.4×10^{-05}	$1.41779826769 \times 10^{00}$	6.0×10^{-07}	$-5.10253549 \times 10^{-06}$	1.4×10^{-10}	-2.174×10^{-12}	0
	1	$1.015988809638 \times 10^{04}$	1.7×10^{-04}	$1.40068325793 \times 10^{00}$	1.7×10^{-06}	$-5.11952998 \times 10^{-06}$	3.1×10^{-10}	-2.174×10^{-12}	0
	2	$1.161720732383 \times 10^{04}$	1.8×10^{-03}	$1.38355285975 \times 10^{00}$	3.7×10^{-06}	$-5.13652446 \times 10^{-06}$	5.0×10^{-10}	-2.174×10^{-12}	0
	3	$1.304847267746 \times 10^{04}$	3.8×10^{-03}	$1.36640707314 \times 10^{00}$	6.5×10^{-06}	$-5.15351895 \times 10^{-06}$	6.9×10^{-10}	-2.174×10^{-12}	0
	4	$1.445365268112 \times 10^{04}$	4.9×10^{-03}	$1.34924589811 \times 10^{00}$	1.0×10^{-05}	$-5.17051344 \times 10^{-06}$	8.8×10^{-10}	-2.174×10^{-12}	0
	5	$1.583267395248 \times 10^{04}$	5.1×10^{-03}	$1.33206933467 \times 10^{00}$	1.4×10^{-05}	$-5.18750792 \times 10^{-06}$	1.0×10^{-09}	-2.174×10^{-12}	0
	6	$1.718542120303 \times 10^{04}$	5.6×10^{-03}	$1.31487738280 \times 10^{00}$	2.0×10^{-05}	$-5.20450241 \times 10^{-06}$	1.2×10^{-09}	-2.174×10^{-12}	0
	7	$1.851173723813 \times 10^{04}$	7.1×10^{-03}	$1.29767004251 \times 10^{00}$	2.7×10^{-05}	$-5.22149690 \times 10^{-06}$	1.4×10^{-09}	-2.174×10^{-12}	0
	8	$1.981142295696 \times 10^{04}$	8.3×10^{-03}	$1.28044731380 \times 10^{00}$	3.4×10^{-05}	$-5.23849138 \times 10^{-06}$	1.6×10^{-09}	-2.174×10^{-12}	0
	9	$2.108423735254 \times 10^{04}$	9.4×10^{-03}	$1.26320919667 \times 10^{00}$	4.2×10^{-05}	$-5.25548587 \times 10^{-06}$	1.8×10^{-09}	-2.174×10^{-12}	0
	10	$2.232989751173 \times 10^{04}$	1.8×10^{-02}	$1.24595569111 \times 10^{00}$	5.2×10^{-05}	$-5.27248035 \times 10^{-06}$	2.0×10^{-09}	-2.174×10^{-12}	0
	11	$2.354807861521 \times 10^{04}$	4.1×10^{-02}	$1.22868679714 \times 10^{00}$	6.2×10^{-05}	$-5.28947484 \times 10^{-06}$	2.2×10^{-09}	-2.174×10^{-12}	0
	12	$2.473841393752 \times 10^{04}$	8.2×10^{-02}	$1.21140251474 \times 10^{00}$	7.3×10^{-05}	$-5.30646933 \times 10^{-06}$	2.4×10^{-09}	-2.174×10^{-12}	0
	13	$2.590049484704 \times 10^{04}$	1.4×10^{-01}	$1.19410284393 \times 10^{00}$	8.5×10^{-05}	$-5.32346381 \times 10^{-06}$	2.6×10^{-09}	-2.174×10^{-12}	0
	14	$2.703387080596 \times 10^{04}$	2.4×10^{-01}	$1.17678778469 \times 10^{00}$	9.8×10^{-05}	$-5.34045830 \times 10^{-06}$	2.8×10^{-09}	-2.174×10^{-12}	0
	15	$2.813804937034 \times 10^{04}$	3.7×10^{-01}	$1.15945733703 \times 10^{00}$	1.1×10^{-04}	$-5.35745279 \times 10^{-06}$	3.0×10^{-09}	-2.174×10^{-12}	0
	16	$2.921249619004 \times 10^{04}$	5.5×10^{-01}	$1.14211150095 \times 10^{00}$	1.2×10^{-04}	$-5.37444727 \times 10^{-06}$	3.2×10^{-09}	-2.174×10^{-12}	0
	17	$3.025663500880 \times 10^{04}$	7.8×10^{-01}	$1.12475027645 \times 10^{00}$	1.4×10^{-04}	$-5.39144176 \times 10^{-06}$	3.4×10^{-09}	-2.174×10^{-12}	0
$b^1\Sigma_g^+$	0	$1.3909328489218 \times 10^{04}$	8.5×10^{-06}	$1.39124930309 \times 10^{00}$	5.1×10^{-08}	$-5.36838562 \times 10^{-06}$	8.1×10^{-11}	-4.503×10^{-12}	0
	1	$1.5314065065520 \times 10^{04}$	3.8×10^{-05}	$1.37296441005 \times 10^{00}$	2.4×10^{-07}	$-5.40197795 \times 10^{-06}$	3.2×10^{-10}	-4.503×10^{-12}	0
	2	$1.6690826016614 \times 10^{04}$	5.0×10^{-04}	$1.35459988936 \times 10^{00}$	1.7×10^{-06}	$-5.43557028 \times 10^{-06}$	6.4×10^{-10}	-4.503×10^{-12}	0
	3	$1.8039535624116 \times 10^{04}$	1.1×10^{-03}	$1.33612562210 \times 10^{00}$	4.5×10^{-06}	$-5.46916260 \times 10^{-06}$	9.6×10^{-10}	-4.503×10^{-12}	0
	4	$1.9360059969662 \times 10^{04}$	2.1×10^{-03}	$1.31751148938 \times 10^{00}$	8.2×10^{-06}	$-5.50275493 \times 10^{-06}$	1.2×10^{-09}	-4.503×10^{-12}	0
	5	$2.0652206934910 \times 10^{04}$	4.0×10^{-03}	$1.29872737230 \times 10^{00}$	1.2×10^{-05}	$-5.53634726 \times 10^{-06}$	1.6×10^{-09}	-4.503×10^{-12}	0
	6	$2.1915726201544 \times 10^{04}$	6.8×10^{-03}	$1.27974315196 \times 10^{00}$	1.8×10^{-05}	$-5.56993959 \times 10^{-06}$	1.9×10^{-09}	-4.503×10^{-12}	0
	7	$2.3150309251268 \times 10^{04}$	1.0×10^{-02}	$1.26052870947 \times 10^{00}$	2.6×10^{-05}	$-5.60353192 \times 10^{-06}$	2.2×10^{-09}	-4.503×10^{-12}	0
	8	$2.4355589365808 \times 10^{04}$	1.3×10^{-02}	$1.24105392591 \times 10^{00}$	3.8×10^{-05}	$-5.63712425 \times 10^{-06}$	2.5×10^{-09}	-4.503×10^{-12}	0
	9	$2.5531141626915 \times 10^{04}$	1.5×10^{-02}	$1.22128868241 \times 10^{00}$	5.5×10^{-05}	$-5.67071658 \times 10^{-06}$	2.8×10^{-09}	-4.503×10^{-12}	0
	10	$2.6676482916361 \times 10^{04}$	1.6×10^{-02}	$1.20120286004 \times 10^{00}$	7.7×10^{-05}	$-5.70430891 \times 10^{-06}$	3.2×10^{-09}	-4.503×10^{-12}	0
	11	$2.7791071915941 \times 10^{04}$	1.6×10^{-02}	$1.18076633992 \times 10^{00}$	1.0×10^{-04}	$-5.73790124 \times 10^{-06}$	3.5×10^{-09}	-4.503×10^{-12}	0
	12	$2.8874309107473 \times 10^{04}$	2.0×10^{-02}	$1.15994900315 \times 10^{00}$	1.4×10^{-04}	$-5.77149357 \times 10^{-06}$	3.8×10^{-09}	-4.503×10^{-12}	0
	13	$2.9925536772797 \times 10^{04}$	3.7×10^{-02}	$1.13872073083 \times 10^{00}$	1.8×10^{-04}	$-5.80508590 \times 10^{-06}$	4.1×10^{-09}	-4.503×10^{-12}	0
	14	$3.0944038993776 \times 10^{04}$	6.6×10^{-02}	$1.11705140406 \times 10^{00}$	2.4×10^{-04}	$-5.83867823 \times 10^{-06}$	4.5×10^{-09}	-4.503×10^{-12}	0
	15	$3.1929041652296 \times 10^{04}$	1.1×10^{-01}	$1.09491090393 \times 10^{00}$	3.0×10^{-04}	$-5.87227055 \times 10^{-06}$	4.8×10^{-09}	-4.503×10^{-12}	0
	16	$3.2879712430264 \times 10^{04}$	1.7×10^{-01}	$1.07226911156 \times 10^{00}$	3.8×10^{-04}	$-5.90586288 \times 10^{-06}$	5.1×10^{-09}	-4.503×10^{-12}	0
	17	$3.3795160809611 \times 10^{04}$	2.5×10^{-01}	$1.04909590803 \times 10^{00}$	4.7×10^{-04}	$-5.93945521 \times 10^{-06}$	5.4×10^{-09}	-4.503×10^{-12}	0

TABLE IV. The spin-splitting constants (in cm^{-1}) for the $X^3\Sigma_g^-$ state of $^{16}O^{16}O$.

v	λ_v	$\sigma\lambda_v$	λ_{Dv}	$\sigma\lambda_{Dv}$	λ_{Hv}	$\sigma\lambda_{Hv}$	λ_{Lv}	$\sigma\lambda_{Lv}$
0	$1.98475142368 \times 10^{00}$	4.0×10^{-08}	$1.9461383 \times 10^{-06}$	2.3×10^{-10}	8.8535×10^{-12}	5.1×10^{-13}	7.223×10^{-16}	3.2×10^{-16}
1	$1.98958040780 \times 10^{00}$	1.0×10^{-07}	$2.0930010 \times 10^{-06}$	5.5×10^{-10}	8.8535×10^{-12}	5.1×10^{-13}	7.223×10^{-16}	3.2×10^{-16}
2	$1.99463074468 \times 10^{00}$	1.1×10^{-05}	$1.9396716 \times 10^{-06}$	1.0×10^{-08}	8.8535×10^{-12}	5.1×10^{-13}	7.223×10^{-16}	3.2×10^{-16}
3	$1.99920969270 \times 10^{00}$	5.8×10^{-05}	$1.4861502 \times 10^{-06}$	2.9×10^{-08}	8.8535×10^{-12}	5.1×10^{-13}	7.223×10^{-16}	3.2×10^{-16}
4	$2.00281000751 \times 10^{00}$	1.6×10^{-04}	$7.3243668 \times 10^{-07}$	5.8×10^{-08}	8.8535×10^{-12}	5.1×10^{-13}	7.223×10^{-16}	3.2×10^{-16}
5	$2.00510994202 \times 10^{00}$	3.3×10^{-04}	$-3.2146892 \times 10^{-07}$	9.7×10^{-08}	8.8535×10^{-12}	5.1×10^{-13}	7.223×10^{-16}	3.2×10^{-16}
6	$2.00597324641 \times 10^{00}$	5.8×10^{-04}	$-1.6755666 \times 10^{-06}$	1.4×10^{-07}	8.8535×10^{-12}	5.1×10^{-13}	7.223×10^{-16}	3.2×10^{-16}
7	$2.00544916810 \times 10^{00}$	9.3×10^{-04}	$-3.3298563 \times 10^{-06}$	2.0×10^{-07}	8.8535×10^{-12}	5.1×10^{-13}	7.223×10^{-16}	3.2×10^{-16}
8	$2.00377245180 \times 10^{00}$	1.3×10^{-03}	$-5.2843382 \times 10^{-06}$	2.6×10^{-07}	8.8535×10^{-12}	5.1×10^{-13}	7.223×10^{-16}	3.2×10^{-16}
9	$2.00136333947 \times 10^{00}$	1.9×10^{-03}	$-7.5390121 \times 10^{-06}$	3.4×10^{-07}	8.8535×10^{-12}	5.1×10^{-13}	7.223×10^{-16}	3.2×10^{-16}
10	$1.99882757033 \times 10^{00}$	2.5×10^{-03}	$-1.0093878 \times 10^{-05}$	4.3×10^{-07}	8.8535×10^{-12}	5.1×10^{-13}	7.223×10^{-16}	3.2×10^{-16}
11	$1.99695638089 \times 10^{00}$	3.2×10^{-03}	$-1.2948936 \times 10^{-05}$	5.2×10^{-07}	8.8535×10^{-12}	5.1×10^{-13}	7.223×10^{-16}	3.2×10^{-16}
12	$1.99672650488 \times 10^{00}$	4.0×10^{-03}	$-1.6104186 \times 10^{-05}$	6.3×10^{-07}	8.8535×10^{-12}	5.1×10^{-13}	7.223×10^{-16}	3.2×10^{-16}
13	$1.99930017333 \times 10^{00}$	4.8×10^{-03}	$-1.9559628 \times 10^{-05}$	7.4×10^{-07}	8.8535×10^{-12}	5.1×10^{-13}	7.223×10^{-16}	3.2×10^{-16}
14	$2.00602511451 \times 10^{00}$	5.7×10^{-03}	$-2.3315262 \times 10^{-05}$	8.6×10^{-07}	8.8535×10^{-12}	5.1×10^{-13}	7.223×10^{-16}	3.2×10^{-16}
15	$2.01843455396 \times 10^{00}$	6.6×10^{-03}	$-2.7371089 \times 10^{-05}$	1.0×10^{-06}	8.8535×10^{-12}	5.1×10^{-13}	7.223×10^{-16}	3.2×10^{-16}
16	$2.03824721449 \times 10^{00}$	7.5×10^{-03}	$-3.1727107 \times 10^{-05}$	1.1×10^{-06}	8.8535×10^{-12}	5.1×10^{-13}	7.223×10^{-16}	3.2×10^{-16}
17	$2.06736731617 \times 10^{00}$	8.4×10^{-03}	$-3.6383318 \times 10^{-05}$	1.2×10^{-06}	8.8535×10^{-12}	5.1×10^{-13}	7.223×10^{-16}	3.2×10^{-16}
18	$2.10788457633 \times 10^{00}$	9.1×10^{-03}	$-4.1339720 \times 10^{-05}$	1.4×10^{-06}	8.8535×10^{-12}	5.1×10^{-13}	7.223×10^{-16}	3.2×10^{-16}
19	$2.16207420956 \times 10^{00}$	9.8×10^{-03}	$-4.6596315 \times 10^{-05}$	1.6×10^{-06}	8.8535×10^{-12}	5.1×10^{-13}	7.223×10^{-16}	3.2×10^{-16}
20	$2.23239692771 \times 10^{00}$	1.0×10^{-02}	$-5.2153102 \times 10^{-05}$	1.8×10^{-06}	8.8535×10^{-12}	5.1×10^{-13}	7.223×10^{-16}	3.2×10^{-16}
21	$2.32149893992 \times 10^{00}$	1.0×10^{-02}	$-5.8010081 \times 10^{-05}$	1.9×10^{-06}	8.8535×10^{-12}	5.1×10^{-13}	7.223×10^{-16}	3.2×10^{-16}
22	$2.43221195256 \times 10^{00}$	1.1×10^{-02}	$-6.4167251 \times 10^{-05}$	2.1×10^{-06}	8.8535×10^{-12}	5.1×10^{-13}	7.223×10^{-16}	3.2×10^{-16}
23	$2.56755316928 \times 10^{00}$	1.1×10^{-02}	$-7.0624614 \times 10^{-05}$	2.4×10^{-06}	8.8535×10^{-12}	5.1×10^{-13}	7.223×10^{-16}	3.2×10^{-16}
24	$2.73072529099 \times 10^{00}$	1.0×10^{-02}	$-7.7382170 \times 10^{-05}$	2.6×10^{-06}	8.8535×10^{-12}	5.1×10^{-13}	7.223×10^{-16}	3.2×10^{-16}
25	$2.92511651586 \times 10^{00}$	1.0×10^{-02}	$-8.4439917 \times 10^{-05}$	2.8×10^{-06}	8.8535×10^{-12}	5.1×10^{-13}	7.223×10^{-16}	3.2×10^{-16}
26	$3.15430053933 \times 10^{00}$	1.0×10^{-02}	$-9.1797856 \times 10^{-05}$	3.0×10^{-06}	8.8535×10^{-12}	5.1×10^{-13}	7.223×10^{-16}	3.2×10^{-16}
27	$3.42203655410 \times 10^{00}$	1.0×10^{-02}	$-9.9455987 \times 10^{-05}$	3.3×10^{-06}	8.8535×10^{-12}	5.1×10^{-13}	7.223×10^{-16}	3.2×10^{-16}
28	$3.73226925013 \times 10^{00}$	1.0×10^{-02}	$-1.0741431 \times 10^{-04}$	3.5×10^{-06}	8.8535×10^{-12}	5.1×10^{-13}	7.223×10^{-16}	3.2×10^{-16}
29	$4.08912881464 \times 10^{00}$	1.2×10^{-02}	$-1.1567282 \times 10^{-04}$	3.8×10^{-06}	8.8535×10^{-12}	5.1×10^{-13}	7.223×10^{-16}	3.2×10^{-16}
30	$4.49693093213 \times 10^{00}$	1.5×10^{-02}	$-1.2423153 \times 10^{-04}$	4.1×10^{-06}	8.8535×10^{-12}	5.1×10^{-13}	7.223×10^{-16}	3.2×10^{-16}
31	$4.96017678435 \times 10^{00}$	2.0×10^{-02}	$-1.3309043 \times 10^{-04}$	4.4×10^{-06}	8.8535×10^{-12}	5.1×10^{-13}	7.223×10^{-16}	3.2×10^{-16}
32	$5.48355305030 \times 10^{00}$	2.6×10^{-02}	$-1.4224952 \times 10^{-04}$	4.7×10^{-06}	8.8535×10^{-12}	5.1×10^{-13}	7.223×10^{-16}	3.2×10^{-16}
33	$6.07193190628 \times 10^{00}$	3.3×10^{-02}	$-1.5170880 \times 10^{-04}$	5.0×10^{-06}	8.8535×10^{-12}	5.1×10^{-13}	7.223×10^{-16}	3.2×10^{-16}
34	$6.73037102581 \times 10^{00}$	4.1×10^{-02}	$-1.6146828 \times 10^{-04}$	5.3×10^{-06}	8.8535×10^{-12}	5.1×10^{-13}	7.223×10^{-16}	3.2×10^{-16}
35	$7.46411357971 \times 10^{00}$	5.1×10^{-02}	$-1.7152795 \times 10^{-04}$	5.6×10^{-06}	8.8535×10^{-12}	5.1×10^{-13}	7.223×10^{-16}	3.2×10^{-16}

O_2 isotopologues. Table S13 in the supplementary material[25] lists the RKR turning points for all six isotopologues. Figure 2 shows the RKR potentials for the main isotopologue, $^{16}O^{16}O$, together with the *ab initio* $X^3\Sigma_g^-$ potential reported by Bytautas *et al.*[21] The quantitative *ab initio* data for $X^3\Sigma_g^-$ were calculated with the CBS+SR+SO+CV parameters listed in Table VII of Bytautas *et al.*;[21] and those for $a^1\Delta_g$ and $b^1\Sigma_g^+$ were taken from Table SII of its supplementary material. The differences plot is generated from an interpolation of the RKR potentials onto the grids of the *ab initio* data points. For the ground state, the agreement between our RKR potential and the *ab initio* one is within 2% for the inner wall from 0.9 Å to 1.2 Å, within 1% for the outer wall from 1.2 Å to 2.0 Å, and up to 5% approaching 2.7 Å. For the $a^1\Delta_g$ state, the difference is 25% at 0.90 Å, 19% at 0.95 Å, 4% at 1.0 Å, within 3% from 1.0 Å to 2.5 Å. For the $b^1\Sigma_g^+$ state, the difference is 17% at 0.90 Å, 8% at 0.95 Å, within 3% from 1.0 Å to 1.3 Å, and within 1% from 1.3 Å to 2.5 Å.

Our RKR potentials and Le Roy's LEVEL8 program[37] were employed to calculate the Franck-Condon factors (FCFs) for the $a^1\Delta_g - X^3\Sigma_g^-$, $b^1\Sigma_g^+ - X^3\Sigma_g^-$, $b^1\Sigma_g^+ - a^1\Delta_g$ band systems. Tables VI–VIII show the results for the main isotopologue, $^{16}O^{16}O$. Table S14 in the supplementary material[25] lists the calculated FCFs for all six isotopologues. Note that in Table S14, (v', J') and (v'', J'') strictly label the upper and lower levels, respectively, and E(lower)=E''. But $E(2) - E(1)$ = (energy of State-2 level)−(energy of State-1 level) where State-2 and State-1 are the two potentials specified in the input file for the LEVEL program. For example, for the $a^1\Delta_g - X^3\Sigma_g^-$system, $a^1\Delta_g$ is State-2 and $X^3\Sigma_g^-$ is State-1; when $E(2) - E(1) > 0$, (v', J') is for $a^1\Delta_g$ and (v'', J'') and E(lower) are for $X^3\Sigma_g^-$; when $E(2) - E(1) < 0$, (v', J') is for $X^3\Sigma_g^-$ and (v'', J'') and E(lower) are for $a^1\Delta_g$.

Our FCFs agree reasonably well with those reported by Nicholls,[23] i.e., for the 0 − 0 band of the $a^1\Delta_g - X^3\Sigma_g^-$, $b^1\Sigma_g^+ - X^3\Sigma_g^-$ and $b^1\Sigma_g^+ - a^1\Delta_g$ systems, the

TABLE V. The spin-rotation constants (in cm^{-1}) for the $X^3\Sigma_g^-$ state of $^{16}O^{16}O$.

v	γ_v	$\sigma\gamma_v$	γ_{Dv}	$\sigma\gamma_{Dv}$	γ_{Hv}	$\sigma\gamma_{Hv}$
0	$-8.425375759 \times 10^{-03}$	2.9×10^{-09}	$-8.130603 \times 10^{-09}$	9.4×10^{-12}	-3.7688×10^{-14}	7.0×10^{-15}
1	$-8.445824185 \times 10^{-03}$	4.3×10^{-09}	$-8.130603 \times 10^{-09}$	9.4×10^{-12}	-3.7688×10^{-14}	7.0×10^{-15}
2	$-8.466272611 \times 10^{-03}$	7.1×10^{-09}	$-8.130603 \times 10^{-09}$	9.4×10^{-12}	-3.7688×10^{-14}	7.0×10^{-15}
3	$-8.486721036 \times 10^{-03}$	1.0×10^{-08}	$-8.130603 \times 10^{-09}$	9.4×10^{-12}	-3.7688×10^{-14}	7.0×10^{-15}
4	$-8.507169462 \times 10^{-03}$	1.3×10^{-08}	$-8.130603 \times 10^{-09}$	9.4×10^{-12}	-3.7688×10^{-14}	7.0×10^{-15}
5	$-8.527617888 \times 10^{-03}$	1.6×10^{-08}	$-8.130603 \times 10^{-09}$	9.4×10^{-12}	-3.7688×10^{-14}	7.0×10^{-15}
6	$-8.548066314 \times 10^{-03}$	2.0×10^{-08}	$-8.130603 \times 10^{-09}$	9.4×10^{-12}	-3.7688×10^{-14}	7.0×10^{-15}
7	$-8.568514739 \times 10^{-03}$	2.3×10^{-08}	$-8.130603 \times 10^{-09}$	9.4×10^{-12}	-3.7688×10^{-14}	7.0×10^{-15}
8	$-8.588963165 \times 10^{-03}$	2.7×10^{-08}	$-8.130603 \times 10^{-09}$	9.4×10^{-12}	-3.7688×10^{-14}	7.0×10^{-15}
9	$-8.609411591 \times 10^{-03}$	3.0×10^{-08}	$-8.130603 \times 10^{-09}$	9.4×10^{-12}	-3.7688×10^{-14}	7.0×10^{-15}
10	$-8.629860017 \times 10^{-03}$	3.3×10^{-08}	$-8.130603 \times 10^{-09}$	9.4×10^{-12}	-3.7688×10^{-14}	7.0×10^{-15}
11	$-8.650308442 \times 10^{-03}$	3.7×10^{-08}	$-8.130603 \times 10^{-09}$	9.4×10^{-12}	-3.7688×10^{-14}	7.0×10^{-15}
12	$-8.670756868 \times 10^{-03}$	4.0×10^{-08}	$-8.130603 \times 10^{-09}$	9.4×10^{-12}	-3.7688×10^{-14}	7.0×10^{-15}
13	$-8.691205294 \times 10^{-03}$	4.3×10^{-08}	$-8.130603 \times 10^{-09}$	9.4×10^{-12}	-3.7688×10^{-14}	7.0×10^{-15}
14	$-8.711653719 \times 10^{-03}$	4.7×10^{-08}	$-8.130603 \times 10^{-09}$	9.4×10^{-12}	-3.7688×10^{-14}	7.0×10^{-15}
15	$-8.732102145 \times 10^{-03}$	5.0×10^{-08}	$-8.130603 \times 10^{-09}$	9.4×10^{-12}	-3.7688×10^{-14}	7.0×10^{-15}
16	$-8.752550571 \times 10^{-03}$	5.4×10^{-08}	$-8.130603 \times 10^{-09}$	9.4×10^{-12}	-3.7688×10^{-14}	7.0×10^{-15}
17	$-8.772998997 \times 10^{-03}$	5.7×10^{-08}	$-8.130603 \times 10^{-09}$	9.4×10^{-12}	-3.7688×10^{-14}	7.0×10^{-15}
18	$-8.793447422 \times 10^{-03}$	6.0×10^{-08}	$-8.130603 \times 10^{-09}$	9.4×10^{-12}	-3.7688×10^{-14}	7.0×10^{-15}
19	$-8.813895848 \times 10^{-03}$	6.4×10^{-08}	$-8.130603 \times 10^{-09}$	9.4×10^{-12}	-3.7688×10^{-14}	7.0×10^{-15}
20	$-8.834344274 \times 10^{-03}$	6.7×10^{-08}	$-8.130603 \times 10^{-09}$	9.4×10^{-12}	-3.7688×10^{-14}	7.0×10^{-15}
21	$-8.854792699 \times 10^{-03}$	7.1×10^{-08}	$-8.130603 \times 10^{-09}$	9.4×10^{-12}	-3.7688×10^{-14}	7.0×10^{-15}
22	$-8.875241125 \times 10^{-03}$	7.4×10^{-08}	$-8.130603 \times 10^{-09}$	9.4×10^{-12}	-3.7688×10^{-14}	7.0×10^{-15}
23	$-8.895689551 \times 10^{-03}$	7.7×10^{-08}	$-8.130603 \times 10^{-09}$	9.4×10^{-12}	-3.7688×10^{-14}	7.0×10^{-15}
24	$-8.916137977 \times 10^{-03}$	8.1×10^{-08}	$-8.130603 \times 10^{-09}$	9.4×10^{-12}	-3.7688×10^{-14}	7.0×10^{-15}
25	$-8.936586402 \times 10^{-03}$	8.4×10^{-08}	$-8.130603 \times 10^{-09}$	9.4×10^{-12}	-3.7688×10^{-14}	7.0×10^{-15}
26	$-8.957034828 \times 10^{-03}$	8.8×10^{-08}	$-8.130603 \times 10^{-09}$	9.4×10^{-12}	-3.7688×10^{-14}	7.0×10^{-15}
27	$-8.977483254 \times 10^{-03}$	9.1×10^{-08}	$-8.130603 \times 10^{-09}$	9.4×10^{-12}	-3.7688×10^{-14}	7.0×10^{-15}
28	$-8.997931680 \times 10^{-03}$	9.4×10^{-08}	$-8.130603 \times 10^{-09}$	9.4×10^{-12}	-3.7688×10^{-14}	7.0×10^{-15}
29	$-9.018380105 \times 10^{-03}$	9.8×10^{-08}	$-8.130603 \times 10^{-09}$	9.4×10^{-12}	-3.7688×10^{-14}	7.0×10^{-15}
30	$-9.038828531 \times 10^{-03}$	1.0×10^{-07}	$-8.130603 \times 10^{-09}$	9.4×10^{-12}	-3.7688×10^{-14}	7.0×10^{-15}
31	$-9.059276957 \times 10^{-03}$	1.0×10^{-07}	$-8.130603 \times 10^{-09}$	9.4×10^{-12}	-3.7688×10^{-14}	7.0×10^{-15}
32	$-9.079725382 \times 10^{-03}$	1.0×10^{-07}	$-8.130603 \times 10^{-09}$	9.4×10^{-12}	-3.7688×10^{-14}	7.0×10^{-15}
33	$-9.100173808 \times 10^{-03}$	1.1×10^{-07}	$-8.130603 \times 10^{-09}$	9.4×10^{-12}	-3.7688×10^{-14}	7.0×10^{-15}
34	$-9.120622234 \times 10^{-03}$	1.1×10^{-07}	$-8.130603 \times 10^{-09}$	9.4×10^{-12}	-3.7688×10^{-14}	7.0×10^{-15}
35	$-9.141070660 \times 10^{-03}$	1.1×10^{-07}	$-8.130603 \times 10^{-09}$	9.4×10^{-12}	-3.7688×10^{-14}	7.0×10^{-15}

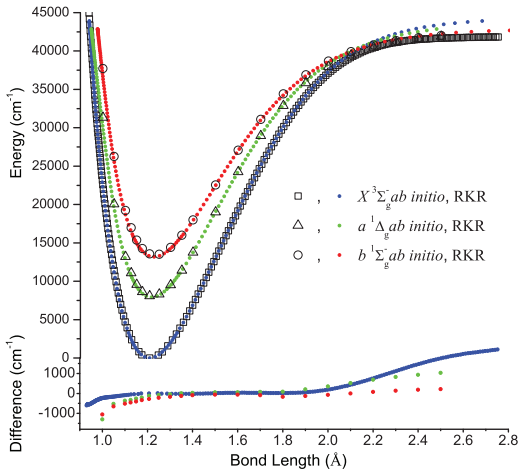

FIG. 2. The RKR potentials of the $X^3\Sigma_g^-$, $a^1\Delta_g$, and $b^1\Sigma_g^+$ states of $^{16}O^{16}O$, together with the *ab initio* $X^3\Sigma_g^-$ potential reported by Bytautas *et al.*[21] and the differences.

obtained values from the current work vs. Nicholls[23] are $\langle 0|0\rangle_{aX} = 0.98688$ vs. 0.98692, $\langle 0|0\rangle_{bX}$ 0.9304 vs. 0.9300, and $\langle 0|0\rangle_{ab}$ 0.97675 vs. 0.97645, respectively. The agreement worsens with increasing v but is still within 50% when the FCFs are larger than 10^{-5}. We view FCFs smaller than 10^{-5} with caution. As is expected for two near-harmonic potentials with similar r_e values, irregular patterns, i.e., oscillatory values in the first row of Table VI, are found in these $\leq 10^{-5}$ numbers. All of the even-v levels are very nearly symmetric, while the odd-v levels are nearly antisymmetric. Thus, the even-v/even-v and odd-v/odd-v vibronic intensities will mainly depend on the overlap with the constant term on the transition moment function and the odd-v/even-v terms with the linear term.

The FCFs of the minor isotopologues differ from those of the main isotopologue, $^{16}O^{16}O$, by a wide range. For example, for the $a^1\Delta_g - X^3\Sigma_g^-$ system, the differences are $\leq$4% when FCF $\geq 10^{-1}$; $\leq$6% when $10^{-2} \leq$ FCF $\leq 10^{-1}$; $\leq$10% when

TABLE VI. Franck-Condon factors for the $^{16}O^{16}O\ a^1\Delta_g - X^3\Sigma_g^-$ band system. The horizontal level designations are v' and the vertical ones are v''.

	0	1	2	3	4	5	6	7	8	9	10
0	9.86888D-01	1.30439D-02	6.81381D-05	6.01330D-10	3.52337D-08	3.70402D-09	2.73387D-10	3.17628D-11	1.35265D-11	1.15542D-11	9.57037D-12
1	1.29854D-02	9.58556D-01	2.81999D-02	2.58182D-04	4.73604D-08	1.57289D-07	2.43938D-08	2.76066D-09	4.91147D-10	2.09094D-10	1.49024D-10
2	1.26355D-04	2.79641D-02	9.25683D-01	4.55801D-02	6.44876D-04	6.41445D-07	4.22234D-07	9.54007D-08	1.51276D-08	3.54588D-09	1.55797D-09
3	3.10972D-07	4.33979D-04	4.50469D-02	8.87959D-01	6.52277D-02	1.32741D-03	3.36922D-06	8.76702D-07	2.87756D-07	6.00050D-08	1.70938D-08
4	5.74816D-09	1.73972D-06	9.95593D-04	6.42807D-02	8.45170D-01	8.71052D-02	2.43264D-03	1.18489D-05	1.53702D-06	7.37537D-07	1.93308D-07
5	2.93318D-11	3.39079D-08	5.89885D-06	1.90593D-03	8.56343D-02	7.97217D-01	1.11081D-01	4.11801D-03	3.31116D-05	2.36034D-06	1.68467D-06
6	5.52543D-12	2.96493D-10	1.26182D-07	1.56721D-05	3.28642D-03	1.08982D-01	7.44141D-01	1.36912D-01	6.57362D-03	7.95637D-05	3.21221D-06
7	4.96091D-12	1.18652D-10	1.59384D-09	3.78420D-07	3.59153D-05	5.29007D-03	1.34086D-01	6.86148D-01	1.64228D-01	1.00233D-02	1.71720D-04
8	5.98884D-12	7.88579D-11	9.41537D-10	6.08160D-09	9.95587D-07	7.44986D-05	8.10607D-03	1.60571D-01	6.23639D-01	1.92513D-01	1.47239D-02
9	4.87031D-12	7.07961D-11	5.68567D-10	4.61102D-09	1.84873D-08	2.39016D-06	1.43822D-04	1.19635D-02	1.87906D-01	5.57246D-01	2.21084D-01
10	3.01034D-12	5.27758D-11	4.39838D-10	2.69663D-09	1.68595D-08	4.75596D-08	5.35117D-06	2.62970D-04	1.71330D-02	2.15383D-01	4.87862D-01
11	1.58540D-12	3.26546D-11	3.10790D-10	1.92593D-09	9.78883D-09	5.05749D-08	1.07288D-07	1.13251D-05	4.60691D-04	2.39241D-02	2.42104D-01
12	7.64713D-13	1.78227D-11	1.93109D-10	1.31719D-09	6.69573D-09	2.94524D-08	1.31414D-07	2.16935D-07	2.28687D-05	7.79401D-04	3.26779D-02
13	3.53512D-13	9.02637D-12	1.08708D-10	8.23568D-10	4.49392D-09	1.97044D-08	7.70392D-08	3.06085D-07	3.98377D-07	4.43599D-05	1.28037D-03
14	1.61131D-13	4.39457D-12	5.74166D-11	4.76411D-10	2.83146D-09	1.30971D-08	5.10469D-08	1.80689D-07	6.53940D-07	6.68851D-07	8.30824D-05
15	7.36708D-14	2.10551D-12	2.92493D-11	2.61029D-10	1.67763D-09	8.32265D-09	3.38064D-08	1.19482D-07	3.88114D-07	1.30241D-06	1.02743D-06
16	3.40486D-14	1.00740D-12	1.46489D-11	1.38329D-10	9.48934D-10	5.03623D-09	2.16745D-08	7.91545D-08	2.57300D-07	7.75020D-07	2.44662D-06
17	1.59570D-14	4.84863D-13	7.29813D-12	7.19924D-11	5.20434D-10	2.92840D-09	1.33611D-08	5.12032D-08	1.70947D-07	5.16516D-07	1.45463D-06
18	7.54364D-15	2.35098D-13	3.63709D-12	3.71471D-11	2.80063D-10	1.65452D-09	7.95664D-09	3.20820D-08	1.11547D-07	3.44700D-07	9.76093D-07
19	3.57867D-15	1.14305D-13	1.81431D-12	1.90857D-11	1.48987D-10	9.16562D-10	4.61251D-09	1.95030D-08	7.08985D-08	2.26813D-07	6.54931D-07
20	1.68519D-15	5.53188D-14	9.02497D-13	9.76403D-12	7.86015D-11	5.00699D-10	2.62036D-09	1.15604D-08	4.38772D-08	1.45993D-07	4.34410D-07
21	7.74171D-16	2.63512D-14	4.44549D-13	4.95447D-12	4.11014D-11	2.70322D-10	1.46497D-09	6.71315D-09	2.65168D-08	9.17745D-08	2.82788D-07
22	3.41111D-16	1.21801D-14	2.14409D-13	2.47557D-12	2.12162D-11	1.44088D-10	8.07154D-10	3.83051D-09	1.56988D-08	5.64170D-08	1.80256D-07
23	1.39729D-16	5.35786D-15	9.96548D-14	1.20432D-12	1.07320D-11	7.55118D-11	4.37665D-10	2.14930D-09	9.12318D-09	3.39847D-08	1.12517D-07
24	4.98503D-17	2.16372D-15	4.35843D-14	5.61074D-13	5.25970D-12	3.86259D-11	2.32590D-10	1.18403D-09	5.20585D-09	2.00855D-08	6.88675D-08
25	1.35725D-17	7.46944D-16	1.72112D-14	2.43969D-13	2.45549D-12	1.90689D-11	1.20290D-10	6.37860D-10	2.91211D-09	1.16473D-08	4.13613D-08
26	1.79419D-18	1.85599D-16	5.65308D-15	9.46190D-14	1.06277D-12	8.93188D-12	5.98858D-11	3.33808D-10	1.59111D-09	6.61716D-09	2.43720D-08
27	7.07529D-20	1.57213D-17	1.24093D-15	2.97735D-14	4.06127D-13	3.86088D-12	2.82246D-11	1.67972D-10	8.44041D-10	3.67147D-09	1.40741D-08
28	1.80186D-18	7.17308D-18	5.21965D-17	5.77504D-15	1.23261D-13	1.46393D-12	1.22544D-11	8.00130D-11	4.30763D-10	1.97930D-09	7.94501D-09
29	4.06778D-18	4.95233D-17	1.40497D-16	7.03488D-17	2.13850D-14	4.35048D-13	4.66143D-12	3.51710D-11	2.08589D-10	1.02888D-09	4.36661D-09
30	5.68147D-18	9.33750D-17	5.88196D-16	1.40218D-15	8.94185D-18	7.03842D-14	1.38923D-12	1.36181D-11	9.37179D-11	5.09834D-10	2.32281D-09
31	6.41011D-18	1.21377D-16	1.00390D-15	4.48192D-15	8.78162D-15	1.03444D-16	2.25974D-13	4.19651D-12	3.75492D-11	2.36526D-10	1.18576D-09
32	6.43524D-18	1.31875D-16	1.25929D-15	7.10980D-15	2.41661D-14	3.82612D-14	2.60207D-16	7.53688D-13	1.23517D-11	9.96361D-11	5.73418D-10
33	5.99053D-18	1.28920D-16	1.34661D-15	8.61937D-15	3.65810D-14	9.82070D-14	1.20273D-13	1.72218D-15	2.65247D-12	3.59151D-11	2.57257D-10
34	5.25761D-18	1.17388D-16	1.30328D-15	9.03408D-15	4.33362D-14	1.45162D-13	3.09778D-13	2.66335D-13	9.12262D-14	9.60100D-12	1.03205D-10
35	4.38663D-18	1.01406D-16	1.17624D-15	8.62796D-15	4.47965D-14	1.69864D-13	4.58020D-13	7.59028D-13	3.57988D-13	1.09842D-12	3.43359D-11

TABLE VII. Franck-Condon factors for the $^{16}O^{16}O$ $b^1\Sigma_g^+ - X^3\Sigma_g^-$ band system. The horizontal level designations are v' and the vertical ones are v''.

	0	1	2	3	4	5	6	7	8	9	10
0	9.30443D-01	6.68051D-02	2.67907D-03	7.20414D-05	1.06665D-06	2.81473D-10	2.21445D-09	4.45407D-10	3.06748D-11	7.00493D-15	1.32272D-12
1	6.69585D-02	7.91611D-01	1.32174D-01	8.88569D-03	3.62443D-04	8.54900D-06	3.63114D-08	9.03597D-09	3.24412D-09	3.45019D-10	5.29035D-12
2	2.54023D-03	1.32959D-01	6.50810D-01	1.93108D-01	1.94204D-02	1.12252D-03	3.90145D-05	4.67558D-07	1.35237D-08	1.22945D-08	2.00719D-09
3	5.75322D-05	8.34154D-03	1.95356D-01	5.12213D-01	2.46248D-01	3.49086D-02	2.73897D-03	1.32977D-04	3.02802D-06	1.74706D-09	3.05140D-08
4	9.75001D-07	2.76928D-04	1.81269D-02	2.51122D-01	3.80622D-01	2.88072D-01	5.56337D-02	5.75602D-03	3.75730D-04	1.36554D-05	6.10787D-08
5	1.17112D-08	6.33388D-06	8.28836D-04	3.25487D-02	2.96975D-01	2.61263D-01	3.15188D-01	8.13360D-02	1.08761D-02	9.28143D-04	4.89077D-05
6	8.04634D-11	1.01297D-07	2.46970D-05	1.97368D-03	5.20832D-02	3.29585D-01	1.59455D-01	3.24744D-01	1.10993D-01	1.89202D-02	2.06733D-03
7	4.55910D-12	9.78965D-10	5.09321D-07	7.48627D-05	4.08729D-03	7.68846D-02	3.45893D-01	8.01053D-02	3.14959D-01	1.42616D-01	3.07228D-02
8	2.23221D-13	4.19002D-11	6.61561D-09	1.94563D-06	1.94239D-04	7.68451D-03	1.06600D-01	3.43558D-01	2.70376D-02	2.85733D-01	1.73135D-01
9	4.58621D-14	1.18883D-12	2.29468D-10	3.28976D-08	6.25551D-06	4.52479D-04	1.34322D-02	1.40151D-01	3.21524D-01	2.15387D-03	2.39270D-01
10	3.32133D-15	2.77660D-13	2.52102D-12	9.86037D-10	1.34485D-07	1.78336D-05	9.72425D-04	2.21378D-02	1.75523D-01	2.80671D-01	4.53401D-03
11	5.64877D-17	6.60617D-15	7.10519D-13	1.26160D-12	3.69715D-09	4.78778D-07	4.64744D-05	1.96038D-03	3.46910D-02	2.09602D-01	2.24427D-01
12	1.27294D-15	1.16522D-14	9.90443D-15	6.94137D-13	3.95448D-12	1.27535D-08	1.53610D-06	1.12859D-04	3.74651D-03	5.19314D-02	2.38184D-01
13	2.24999D-15	3.60934D-14	2.44822D-13	7.62811D-13	1.22558D-14	1.15432D-10	4.16456D-08	4.54022D-06	2.58638D-04	6.83276D-03	7.44111D-02
14	2.62492D-15	4.88522D-14	4.37878D-13	2.39709D-12	8.54197D-12	8.38774D-12	9.07659D-10	1.30688D-07	1.25472D-05	5.64079D-04	1.19383D-02
15	2.57197D-15	5.12057D-14	5.07889D-13	3.28641D-12	1.51793D-11	5.30374D-11	7.47049D-11	4.64116D-09	3.96924D-07	3.27555D-05	1.17723D-03
16	2.26782D-15	4.72221D-14	4.93961D-13	3.44237D-12	1.77739D-11	7.13318D-11	2.35611D-10	3.39339D-10	1.88543D-08	1.16955D-06	8.13608D-05
17	1.85766D-15	4.00161D-14	4.34439D-13	3.16224D-12	1.72887D-11	7.51531D-11	2.67709D-10	8.30486D-10	1.07119D-09	6.62380D-08	3.34278D-06
18	1.42381D-15	3.17431D-14	3.55421D-13	2.67200D-12	1.51573D-11	6.89925D-11	2.61144D-10	8.39194D-10	2.45534D-09	2.56283D-09	2.10830D-07
19	1.03512D-15	2.37296D-14	2.73660D-13	2.11609D-12	1.23576D-11	5.80962D-11	2.28534D-10	7.71042D-10	2.26411D-09	6.30752D-09	4.67480D-09
20	7.08752D-16	1.67815D-14	1.99046D-13	1.58204D-12	9.48689D-12	4.58202D-11	1.85592D-10	6.47441D-10	1.98120D-09	5.37127D-09	1.44444D-08
21	4.57171D-16	1.11803D-14	1.36767D-13	1.11792D-12	6.88548D-12	3.41232D-11	1.41837D-10	5.08503D-10	1.60351D-09	4.51146D-09	1.13869D-08
22	2.76359D-16	6.98535D-15	8.83020D-14	7.44699D-13	4.72020D-12	2.40327D-11	1.02507D-10	3.77018D-10	1.22060D-09	3.53137D-09	9.23728D-09
23	1.52743D-16	4.04005D-15	5.31099D-14	4.64208D-13	3.04144D-12	1.59613D-11	7.00249D-11	2.64508D-10	8.78863D-10	2.61004D-09	7.01129D-09
24	7.50754D-17	2.11031D-15	2.92308D-14	2.67357D-13	1.82371D-12	9.92565D-12	4.50022D-11	1.75201D-10	5.98807D-10	1.82692D-09	5.04080D-09
25	3.11180D-17	9.54661D-16	1.42513D-14	1.38896D-13	1.00010D-12	5.70391D-12	2.69508D-11	1.08846D-10	3.84560D-10	1.20967D-09	3.43419D-09
26	9.23376D-18	3.38895D-16	5.76711D-15	6.21786D-14	4.85489D-13	2.95954D-12	1.47875D-11	6.26574D-11	2.30819D-10	7.53494D-10	2.21205D-09
27	1.00238D-18	6.91378D-17	1.63262D-15	2.16335D-14	1.95149D-13	1.32547D-12	7.20771D-12	3.27026D-11	1.27526D-10	4.36908D-10	1.33775D-09
28	3.01530D-19	2.06341D-19	1.50205D-16	4.20629D-15	5.46417D-14	4.63179D-13	2.92989D-12	1.48533D-11	6.30915D-11	2.31481D-10	7.49914D-10
29	2.76662D-18	2.90125D-17	8.37700D-17	1.17841D-18	4.85250D-15	9.20069D-14	8.46776D-13	5.36410D-12	2.64659D-11	1.08250D-10	3.81084D-10
30	5.87622D-18	9.01071D-17	6.06536D-16	2.13426D-15	2.99821D-15	1.35527D-16	8.84455D-14	1.17984D-12	8.25529D-12	4.15604D-11	1.68224D-10
31	8.40671D-18	1.47733D-16	1.23021D-15	6.28206D-15	2.08619D-14	4.16965D-14	3.02919D-14	1.86420D-14	1.18324D-12	1.07917D-11	5.86635D-11
32	9.82456D-18	1.85775D-16	1.71175D-15	1.00903D-14	4.19048D-14	1.25961D-13	2.64054D-13	3.20978D-13	7.00772D-14	7.08388D-13	1.21130D-11
33	1.00683D-17	2.00483D-16	1.96662D-15	1.25510D-14	5.80175D-14	2.03854D-13	5.51700D-13	1.12183D-12	1.54552D-12	9.48294D-13	9.22927D-14
34	9.41202D-18	1.95353D-16	2.00366D-15	1.34797D-14	6.65217D-14	2.54596D-13	7.76503D-13	1.89787D-12	3.64061D-12	5.09081D-12	4.04553D-12
35	8.23858D-18	1.76799D-16	1.87654D-15	1.31259D-14	6.78106D-14	2.74457D-13	8.99216D-13	2.42299D-12	5.37242D-12	9.60524D-12	1.30107D-11

TABLE VIII. Franck-Condon factors for the $^{16}O^{16}O\ a^1\Delta_g - b^1\Sigma_g^+$ band system. The horizontal level designations are v' and the vertical ones are v''.

	0	1	2	3	4	5	6	7	8	9	10
0	9.76752D-01	2.28700D-02	3.73084D-04	4.81199D-06	3.63123D-08	2.38233D-12	3.96175D-11	1.85037D-13	6.08627D-12	1.10862D-11	1.04809D-11
1	2.30329D-02	9.28359D-01	4.73326D-02	1.25152D-03	2.38156D-05	2.83890D-07	4.74961D-10	5.14843D-11	1.34861D-11	9.68812D-11	1.30621D-10
2	2.14377D-04	4.80475D-02	8.75685D-01	7.31870D-02	2.79116D-03	7.34404D-05	1.29599D-06	9.53933D-09	3.58032D-11	3.10647D-10	7.20044D-10
3	6.78576D-07	7.20158D-04	7.49854D-02	8.18751D-01	1.00183D-01	5.17456D-03	1.80575D-04	4.48550D-06	7.20966D-08	2.36542D-09	2.44602D-09
4	2.05181D-09	3.39408D-06	1.61296D-03	1.03766D-01	7.57611D-01	1.27993D-01	8.61309D-03	3.87151D-04	1.30026D-05	3.51345D-07	2.05754D-08
5	1.42665D-13	1.21056D-08	1.06741D-05	3.01216D-03	1.34264D-01	6.92389D-01	1.56186D-01	1.33466D-02	7.56143D-04	3.32321D-05	1.31839D-06
6	1.19513D-12	5.20429D-11	4.32487D-08	2.69704D-05	5.06721D-03	1.66282D-01	6.23341D-01	1.84183D-01	1.96385D-02	1.37917D-03	7.72268D-05
7	4.55331D-12	3.89502D-11	6.39914D-10	1.22201D-07	5.98063D-05	7.96483D-03	1.99508D-01	5.50910D-01	2.11227D-01	2.77639D-02	2.38567D-03
8	4.90930D-12	5.67124D-11	3.47062D-10	3.66320D-09	3.02662D-07	1.21499D-04	1.19369D-02	2.33476D-01	4.75809D-01	2.36343D-01	3.79863D-02
9	3.36890D-12	5.05229D-11	3.50753D-10	1.75545D-09	1.42497D-08	6.92475D-07	2.31718D-04	1.72684D-02	2.67508D-01	3.99105D-01	2.58315D-01
10	1.84163D-12	3.35144D-11	2.78114D-10	1.47736D-09	6.35895D-09	4.35689D-08	1.50794D-06	4.21232D-04	2.43031D-02	3.00661D-01	3.22304D-01
11	8.80820D-13	1.85666D-11	1.79975D-10	1.08582D-09	4.82231D-09	1.83699D-08	1.12800D-07	3.18059D-06	7.37341D-04	3.34465D-02	3.31672D-01
12	3.84902D-13	9.12910D-12	1.00618D-10	6.89298D-10	3.36409D-09	1.30661D-08	4.49092D-08	2.58560D-07	6.56282D-06	1.25163D-03	4.51589D-02
13	1.56239D-13	4.10511D-12	5.04759D-11	3.87383D-10	2.10166D-09	8.77667D-09	3.06352D-08	9.63583D-08	5.40608D-07	1.33161D-05	2.07079D-03
14	5.87480D-14	1.70379D-12	2.31556D-11	1.96924D-10	1.18292D-09	5.40465D-09	1.99903D-08	6.38782D-08	1.85859D-07	1.05383D-06	2.66270D-05
15	1.99449D-14	6.46565D-13	9.73457D-12	9.14325D-11	6.05604D-10	3.03599D-09	1.21406D-08	4.07145D-08	1.20732D-07	3.27675D-07	1.94869D-06

$10^{-3} \leq$ FCF $\leq 10^{-2}$; $\leq$12% when $10^{-4} \leq$ FCF $\leq 10^{-3}$; and $\leq$40% when $10^{-5} \leq$ FCF $\leq 10^{-4}$.

VII. CONCLUSIONS

We have continued developing a comprehensive model for oxygen quantum states below 16,000 cm^{-1} based on experimental data and shown that a variety of "useful" products may be systematically derived from the model. The isotope independent Dunham parameters have impressive predictive powers that may be under-utilized without the precise and methodical application of mathematical algorithms such as SPCAT and LEVEL. Using these tools we have derived "useful" quantities such as energy levels, partition sums, band constants, RKR turning points, and Franck-Condon factors.[38]

The determination of energy levels is inherent to the process of fitting transition frequencies of measured transitions. Here we have utilized the predictive power of the model to extend the energy level determinations beyond the measurements such that new vibronic and/or isotopic bands are readily identifiable. Comparisons of the energy levels and transitions among them with existing data compilations[29] have revealed only minor inconsistencies; however, the coverage of existing data compilations is limited to just a few vibronic states and two of the five minor isotopologues. We anticipate that future measurements will reveal the true predictive power of the isotope independent Dunham model and we note that measurements that deviate from the predictions given here will be the most useful for improvement of the model.

The energy levels derived in this work are immediately useful for the generation of accurate and precise partition sums for each isotopologue. Again, comparison with existing sources[30] have revealed minor inconsistencies. We recommend that any intensities derived using $O^{18}O$ or $O^{17}O$ partition sums from Ref. 30 be re-evaluated since the discrepancies will introduce systematic errors on the order of 1% if they are used in combination with the updated TIPS values.[31]

When new researches on oxygen bands are analyzed, it is likely that band parameters will be reported. The inherent difficulties associated with comparisons between simple and extensive models motivated us to report derived band parameters from our model. The band parameters from this work give future researchers a direct metric to compare both the precision and accuracy of the new measurements with our grand fit.

Additionally, we have shown that experimental RKR potentials are in agreement with *ab initio* results within the range of experimental data. The difference near the inner and outer extrema of the data reveal just a few percent deviation from theory. Since our RKR inversion of the isotope independent Dunham model does not explicitly treat the spin-couplings among the potentials, but rather incorporates effective, isolated, potentials, we do not expect the potentials to display the spin-orbit induced crossing as the molecule approaches dissociation.[21] These potentials are useful for generation of the Franck-Condon factors that meter the intensities of vibronic bands within a pair of potentials, and we have uti-

lized them to generate a comprehensive listing for states below 16 000 cm^{-1} and all six isotopologues.

We anticipate improvements to energy levels and other derived parameters will come from high precision spectroscopic techniques applied to previously unmeasured vibronic and isotopic bands. Extensions of experimental data sets to high lying vibronic states could significantly improve the accuracy of the RKR potentials. We intend to update our model accordingly as new research is published. We also have begun the process of determining the various transition moments required for generation of intensities for the transitions within and among these oxygen states.

ACKNOWLEDGMENTS

We would like to thank Dr. Iouli Gordon for helpful discussions. We are grateful to Professor Robert Le Roy for helpful discussion on using his RKR and LEVEL programs. The research described in this paper was performed at the Jet Propulsion Laboratory, California Institute of Technology, under contract with the National Aeronautics and Space Administration.

[1] D. O'Brien and R. Mitchell, J. Appl. Meterol. **31**, 1179 (1992).
[2] D. Tarasick and W. Evans, Adv. Space Res. **13**(1), 145 (1993).
[3] M. Mlynczak and D. Olander, Geophys. Res. Lett. **22**, 1377, doi:10.1029/95GL01321 (1995).
[4] T. Slanger, D. Huestis, D. Osterbrock, and J. Fulbright, Science **277**, 1485 (1997).
[5] D. O'Brien, S. English, and G. Costa, J. Atmos. Oceanic Technol. **14**, 105 (1997).
[6] D. O'Brien, R. Mitchell, S. English, and G. Costa, J. Atmos. Oceanic Technol. **15**, 1272 (1998).
[7] A. Heidinger and G. L. Stephens, J. Atmos. Sci. **57**, 1615 (2000).
[8] M. Mlynczak, F. Morgan, J.-H. Yee, P. Espy, D. Murtagh, B. Marshall, and F. Schmidlin, Geophys. Res. Lett. **28**, 999, doi:10.1029/2000GL012423 (2001).
[9] R. Clancy, B. Sandor, M. Wolff, M. Smith, F. Lefevre, J. Madeleine *et al.*, J. Geophys. Res.: Planets **118**, 1148, doi:10.1002/jgre.20073 (2013).
[10] T. Slanger, N. Chanover, B. Sharpee, and T. Bida, Icarus **217**, 845 (2012).
[11] R. Liseau, P. Goldsmith, B. Larsson, L. Pagani, P. Bergman, J. L. Bourlot *et al.*, Astron. Astrophys. **541**, A73 (2012).
[12] U. Yildiz, K. Acharyya, P. Goldsmith, E. van Dishoeck, G. Melnick, R. Snell *et al.*, Astron. Astrophys. **558**, A58 (2013).
[13] A. Kuze, H. Suto, M. Nakajima, and T. Hamazaki, Appl. Opt. **48**, 6716 (2009).
[14] D. Crisp, B. Fisher, C. O'Dell, C. Frankenberg, R. Basilio, H. Boesch, L. Brown, R. Castano, B. Connor, N. Deutscher, A. Eldering, D. Griffith, M. Gunson, A. Kuze, L. Mandrake, J. McDuffie, J. Messerschmidt, C. Miller, I. Morino, V. Natraj, J. Notholt, D. O'Brien, F. Oyafuso, I. Polonsky, J. Robinson, R. Salawitch, V. Sherlock, M. Smyth, H. Suto, T. Taylor, D. Thompson, P. Wennberg, D. Wunch, and Y. Yung, Atmos. Meas. Tech. **5**, 687 (2012).
[15] W. Chen, Y. Zhang, X. Yin, C. Yan, Z. Yang, and Y. Liu, *Proceedings of the 63rd International Astronautical Congress, Naples, Italy*, 2012.
[16] S. Yu, C. Miller, B. Drouin, and H. Muller, J. Chem. Phys. **137**, 024304 (2012).
[17] B. Drouin, H. Gupta, S. Yu, C. Miller, and H. Muller, J. Chem. Phys. **137**, 024305 (2012).
[18] B. Drouin, S. Yu, B. Elliott, T. Crawford, and C. Miller, J. Chem. Phys. **139**, 144301 (2013).
[19] O. Leshchishina, S. Kassi, I. Gordon, L. Rothman, L. Wang, and A. Campargue, J. Quantum Spectrosc. Radiat. Transfer **111**, 2236 (2010).
[20] D. Robichaud, J. Hodges, L. Brown, D. Lisak, P. Maslowski, L. Yeung, M. Okumura, and C. Miller, J. Molec. Spectrosc. **248**, 1 (2008).
[21] L. Bytautas, N. Matsunaga, and K. Ruedenberg, J. Chem. Phys. **132**, 074307 (2010).
[22] B. Minaev, Spectrochim. Acta A **60**, 1027 (2004).
[23] R. Nicholls, J. Res. Natl. Bur. Stand. A **69A**, 369 (1965).
[24] H. Pickett, J. Mol. Spectrosc. **148**, 371 (1991).
[25] See supplementary material at http://dx.doi.org/10.1063/1.4900510 for (1) the SPFIT input and output files of the updated O_2 Dunham model; (2) Table S1 for the energy levels of $X^3\Sigma_g^-$, $a^1\Delta_g$ and $b^1\Sigma_g^+$ of $^{16}O^{16}O$ and Tables S2-S6 for those of $^{16}O^{17}O$, $^{16}O^{18}O$, $^{17}O^{17}O$, $^{17}O^{18}O$ and $^{18}O^{18}O$; (3) Table S7 for the hyperfine-free energy levels of $X^3\Sigma_g^-$, $a^1\Delta_g$ and $b^1\Sigma_g^+$ of $^{16}O^{17}O$, and Tables S8-S9 for those of $^{17}O^{17}O$ and $^{17}O^{18}O$; (4) Table S10 for the band constants of $X^3\Sigma_g^-$ of all six O_2 isotopologues, and Tables S11-S12 for those of $a^1\Delta_g$ and $b^1\Sigma_g^+$; (6) Table S13 for RKR turning points for $X^3\Sigma_g^-$, $a^1\Delta_g$ and $b^1\Sigma_g^+$ of six O_2 isotopologues; (7) Table S14 for Franck-Condon factors for the $a^1\Delta_g - X^3\Sigma_g^-$, $b^1\Sigma_g^+ - X^3\Sigma_g^-$, $b^1\Sigma_g^+ - a^1\Delta_g$ band systems of six O_2 isotopologues.
[26] H. Edwards, D. Long, and K. Najm, J. Raman Spectrosc. **17**, 431 (1986).
[27] J. Brown, J. Hougen, K. Huber, J. Johns, I. Kopp, H. Lefebvre-Brion, A. Merer, D. Ramsay, J. Rostas, and R. Zare, J. Mol. Spectrosc. **55**, 500 (1975).
[28] G. Cazzolli, C. D. Esposti, and B. Landsberg, IL Nuovo Cimento **3**, 341 (1984).
[29] L. Rothman, I. Gordon, Y. Babikov, A. Barbe, D. Benner, P. Bernath, M. Birk, L. Bizzocchi, V. Boudon, L. Brown, A. Campargue, K. Chance, E. Cohen, L. Coudert, V. Devi, B. Drouin, A. Fayt, J.-M. Flaud, R. Gamache, J. Harrison, J.-M. Hartmann, C. Hill, J. Hodges, D. Jacquemart, A. Jolly, J. Lamouroux, R. L. Roy, G. Li, D. Long, O. Lyulin, C. Mackie, S. Massie, S. Mikhailenko, H. Mueller, O. Naumenko, A. Nikitin, J. Orphal, V. Perevalov, A. Perrin, E. Polovtseva, C. Richard, M. Smith, E. Starikova, K. Sung, S. Tashkun, J. Tennyson, G. Toon, V. Tyuterev, and G. Wagner, J. Quantum Spectrosc. Radiat. Transfer **130**, 4 (2013).
[30] J. Fischer, R. Gamache, A. Goldman, L. Rothman, and A. Perrin, J. Quantum Spectrosc. Radiat. Transfer **82**, 401 (2003).
[31] R. Gamache, private communication (2014).
[32] P. J. Mohr, B. N. Taylor, and D. B. Newell, Rev. Mod. Phys. **84**, 1527 (2012).
[33] D. Long, D. Havey, M. Okumura, H. Pickett, C. Miller, and J. Hodges, Phys. Rev. A **80**, 042513 (2009).
[34] D. Long, D. Havey, S. Yu, M. Okumura, C. Miller, and J. Hodges, J. Quantum Spectrosc. Radiat. Transfer **112**, 2527 (2011).
[35] B. Minaev, Opt. Spektrosk. **45**, 1202 (1978).
[36] R. J. Le Roy, RKR1 2.0, A computer program implementing the first-order RKR method for determining diatomic molecule potential energy function, University of Waterloo, Chemical Physics Research Report No. CP-657R, 2004, see http://leroy.uwaterloo.ca/programs.
[37] R. J. Le Roy, LEVEL 8.0, A computer program for solving the radial Schrodinger equation for bound and quasibound levels, University of Waterloo, Chemical Physics Research Report No. CP-663, 2007, see http://leroy.uwaterloo.ca/programs.
[38] P. Krupenie, J. Phys. Chem. Ref. Data **1**, 423 (1972).